Research Square

Preprints are preliminary reports that have not undergone peer review.
They should not be considered conclusive, used to inform clinical practice,
or referenced by the media as validated information.

Feasibility-and connected-domain-guided multi-objective particle swarm optimization for multi-loop mechanism synthesis

Ran Cheng
Beijing Institute of Precision Mechatronics and Controls
Zhiyuan Yu
Beijing Institute of Precision Mechatronics and Controls
Hongzhou Song
451345842@qq.com

Beijing Institute of Precision Mechatronics and Controls
Shihao Mao
Beijing Institute of Precision Mechatronics and Controls
Zixing Wang
Beijing Institute of Precision Mechatronics and Controls

Article

Keywords: multi-loop mechanism synthesis, constrained multi-objective optimization, feasible input-domain connectivity, multi-objective particle swarm optimization, archive maintenance, inverse-dynamics verification

Posted Date: June 24th, 2026

DOI: https://doi.org/10.21203/rs.3.rs-9930739/v1

License: This work is licensed under a Creative Commons Attribution 4.0 International License.
Read Full License

Additional Declarations: No competing interests reported.

Feasibility-and connected-domain-guided multi-objective particle swarm optimization for multi-loop mechanism synthesis

Ran Cheng[1,2], **Zhiyuan Yu**[1,2], **Hongzhou Song**[1,2,*], **Shihao Mao**[1,2], **and Zixing Wang**[1,2]

[1]Beijing Institute of Precision Mechatronics and Controls, Beijing 100076, China
[2]Innovation Center for Control Actuators, Beijing 100076, China
[*]451345842@qq.com

ABSTRACT

Dimensional synthesis of multi-loop mechanisms must satisfy loop closure, branch continuity, singularity margin, task coverage and load transfer requirements. Penalty-based treatment is inefficient for fragmented feasible input domains under limited evaluations. This study formulates constrained sizing as a two-objective search that minimizes task-coverage error and a clipped load proxy, while using connected-domain quality as internal guidance. A feasibility- and connected-domain-guided multi-objective particle swarm optimizer (FCD-MOPSO) is proposed, combining mechanism-aware input-space evaluation, feasibility-first comparison, connected-domain-guided archive maintenance, mixed leader selection and bounded perturbation. Under a soft-constrained low-budget protocol, FCD-MOPSO increased the valid-run rate from 0.6 to 0.8 and the high-quality (HQ) and force-aware HQ rates from 0.1 to 0.4 relative to Basic MOPSO. Search histories showed earlier archive formation and more consistent coverage accumulation. Representative inverse-dynamics verification showed lower peak force, RMS force, force-gradient risk and smoothness index than selected Basic MOPSO and PSO representatives. Strict-feasibility diagnosis identified coverage pressure as the limiting factor. FCD-MOPSO is positioned as a mechanism-aware screening optimizer for fragmented feasible active-input domains.

Keywords: multi-loop mechanism synthesis, constrained multi-objective optimization, feasible input-domain connectivity, multi-objective particle swarm optimization, archive maintenance, inverse-dynamics verification

Introduction

Multi-loop and parallel mechanisms are used in robotic manipulators, precision positioning platforms, reconfigurable structures and compact actuation systems because closed-loop transmission paths can provide high stiffness, high load capacity and compact force flow. Their dimensional synthesis is more constrained than that of open-chain mechanisms. For a fixed topology, the attainable output set is jointly determined by active inputs, loop-closure equations, passive-branch selection, assembly limits and singular configurations. Singularity analysis based on constraint equations and Jacobian properties has therefore become a basic tool for closed-loop mechanism evaluation, together with condition-number indices, global performance measures and singularity-free workspace descriptions[1–5].

In mechanism synthesis, difficulty arises from both the number of design variables and the discontinuous mapping between dimensions, active inputs and feasible outputs. A small change in link length can remove a closure solution, switch an assembly branch or move a trajectory close to a singular boundary. Classical manipulability and Jacobian-based indices provide local performance information[6], whereas task-envelope synthesis additionally requires global reasoning over a finite input domain and over the reachable output set. For compact morphing or reconfigurable mechanisms, this distinction is important because the design must maintain continuous operation over a mission envelope rather than only satisfying isolated precision poses.

Dimensional synthesis of parallel mechanisms has been studied through workspace, dexterity, stiffness, velocity transmission, force transmission and dynamic-performance criteria. Representative studies include well-shaped workspace design for two-degree-of-freedom planar parallel manipulators[7], prescribed-workspace optimization for spherical parallel manipulators[8], multi-objective dimensional design of linear Delta robots[9], and kinematic-dynamic dexterity optimization of spherical parallel mechanisms[10]. More recent work has extended this line to artificial-intelligence-based manipulator design, general 6-PUS parallel manipulators, performance-optimization reviews, double-driven parallel mechanisms, parallel-serial architectures and bilevel or hierarchical dimensional synthesis[11–17]. Mechanisms with sub-closed loops, double-driven chains and redundant closed-loop structures further increase the difficulty of kinematic modeling, error propagation and multi-objective optimization[18–20].

These studies reveal a common computational structure. The dimensional variables are optimized outside the inner kinematic and dynamic solvers, so each candidate design must be evaluated by an expensive numerical pipeline. The pipeline may include loop-closure solution, workspace sampling, condition-number calculation, force transmission estimation, dynamic checking and engineering screening. Such a pipeline is compatible with population-based optimization, but it makes each function evaluation valuable. A low-budget algorithm therefore needs to use intermediate mechanism information more effectively than a black-box objective value alone.

Particle swarm optimization (PSO), genetic algorithms and multi-objective evolutionary algorithms have been widely adopted for non-convex, non-differentiable and multimodal engineering design problems. PSO updates particles through individual and social learning terms[21,22]. NSGA-II introduced fast non-dominated sorting, crowding distance and elitist preservation[23]. Multi-objective particle swarm optimization (MOPSO) introduced Pareto dominance and an external archive into PSO, enabling archive-based leader selection for multi-objective search[24,25]. Subsequent studies have improved MOPSO through archive maintenance, leader selection, adaptive parameters, mutation or perturbation, diversity preservation and constraint handling[26–31]. Recent Scientific Reports studies also show that archive-guided mutation, angular segmentation, dynamic updating and hierarchical reference-point maintenance remain active directions for MOPSO development[32–34].

For constrained multi-objective optimization, two issues are especially relevant here. First, constraint handling must determine whether an infeasible point with promising objective values should be retained, repaired or discarded[29–31]. Second, the quality of an approximate Pareto set is usually judged through convergence and diversity indicators such as hypervolume[35,36]. In a mechanism-derived problem, however, an objective-space non-dominated point can still correspond to an input-space domain that is fragmented, branch-discontinuous or close to singularity. Objective-space indicators should therefore be complemented by mechanism-domain indicators when the optimizer is used for dimensional synthesis.

This behavior is particularly harmful in archive-based MOPSO. The archive records final solutions and supplies the leaders used in subsequent particle updates. Once invalid or weakly connected candidates influence the archive, the social learning term may repeatedly pull particles toward regions that look acceptable in objective space but are difficult to execute in the active-input space. A more appropriate strategy is to let the input-domain state map influence candidate comparison, archive truncation and leader selection directly.

This study proposes feasibility- and connected-domain-guided multi-objective particle swarm optimization (FCD-MOPSO) for mechanism-derived constrained synthesis problems. The method keeps the basic MOPSO movement equations but embeds feasible-input ratio, largest connected-component ratio, task-envelope coverage, path-connectivity information and load-proxy risk into particle evaluation, personal-best updating, archive maintenance and leader selection. The contribution is threefold. First, a constrained bi-objective sizing formulation is established for task-envelope coverage error and clipped load-proxy minimization while retaining connected-domain quality as a search-guidance metric. Second, a mechanism-aware FCD-MOPSO framework is developed by combining feasibility-first hierarchical comparison, adaptive soft-constraint weighting, connected-domain-guided archive maintenance, mixed leader selection and local perturbation. Third, the method is evaluated through a mechanism-derived constrained benchmark, input-domain risk diagnosis, neighboring stress settings, ablation analysis and representative inverse-dynamics verification. The experimental interpretation is deliberately restricted to soft-constrained low-budget search stability and representative engineering-risk reduction, so strict-feasibility certification is not claimed from the low-budget diagnostic protocol.

The remainder of the article is organized as follows. The Methods section defines the mechanism-derived constrained sizing model, the FCD-MOPSO workflow, the archive and leader strategies, and the verification protocol. The Results section reports input-domain diagnosis, low-budget benchmark comparisons, stress-setting behavior, ablation results and representative inverse-dynamics verification. The Discussion interprets the scope and limitations of the evidence, and the Conclusion summarizes the final findings.

Methods

Overall FCD-MOPSO workflow

The proposed framework uses the same particle-position, velocity, personal-best and archive concepts as Basic MOPSO, but changes the information passed through these objects. Figure 1 summarizes the complete search loop and the following subsections formalize its components. Each particle is treated as a dimension vector. It is evaluated by scanning the active-input space, solving the loop-closure equations, classifying input samples and computing mechanism-domain descriptors. These descriptors are then used in three algorithmic decisions: feasibility-first comparison for personal-best updating, connected-domain-guided archive retention, and mixed connected-domain/diversity leader selection. Local perturbation is applied around promising candidates to improve sampling near narrow feasible-domain boundaries.

Mechanism-aware evaluation forms the front-end stage of the method (Fig. 2). A candidate design is not judged only by the final objective vector. Instead, the active-input grid is scanned to determine loop-closure solvability, geometric validity, branch continuity, singularity risk, usable connected components and load-proxy distribution. This state map is converted into

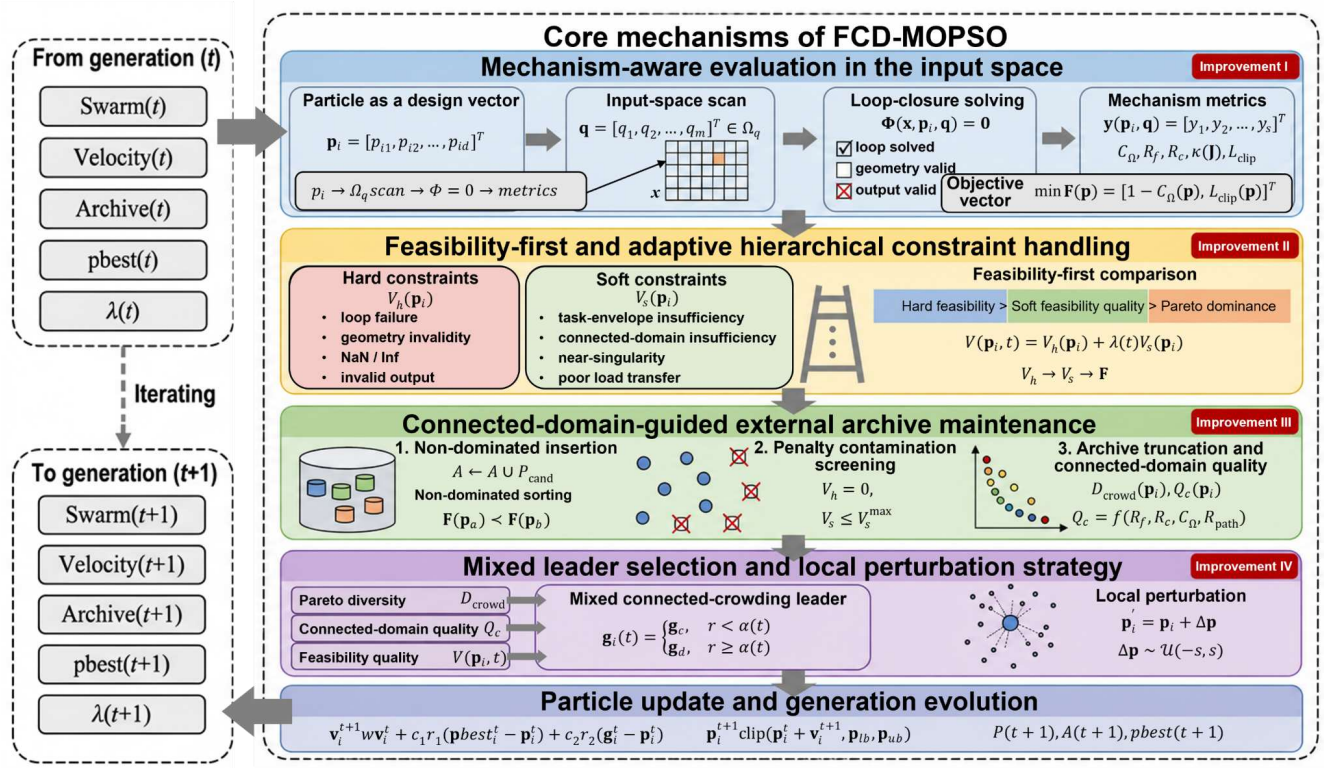


Figure 1. Core mechanisms of FCD-MOPSO.

hard violation score V_{h}, soft violation score V_{s}, task coverage $C_{\chi A}$, largest connected-component ratio R_{c}, path-connectivity descriptor R_{path} and connected-domain quality Q_{c}. The distinction between hard and soft violations is important: loop-closure failure or invalid geometry prevents meaningful objective interpretation, whereas moderate coverage shortage or near-boundary singularity margin can still guide the search under a stress-test protocol.

The archive and leader strategy is shown in Fig. 3. Ordinary non-dominated sorting is retained, but candidate retention is no longer determined by objective-space crowding alone. Archive points with higher connected-domain quality are protected after hard-infeasible and penalty-contaminated candidates have been filtered. The leader used by a particle alternates between a diversity leader and a connected-domain leader. This design reduces the probability that the social term repeatedly pulls the swarm toward an objective-space attractive but input-space fragmented region.

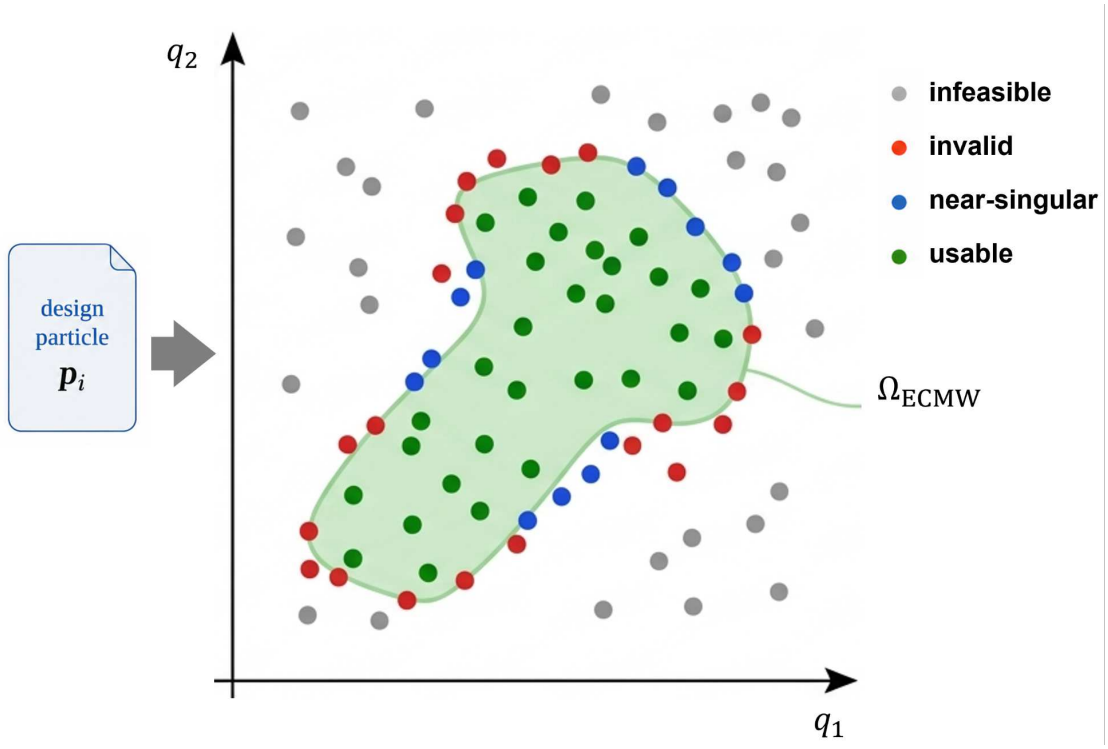


Figure 2. Mechanism-aware evaluation strategy.

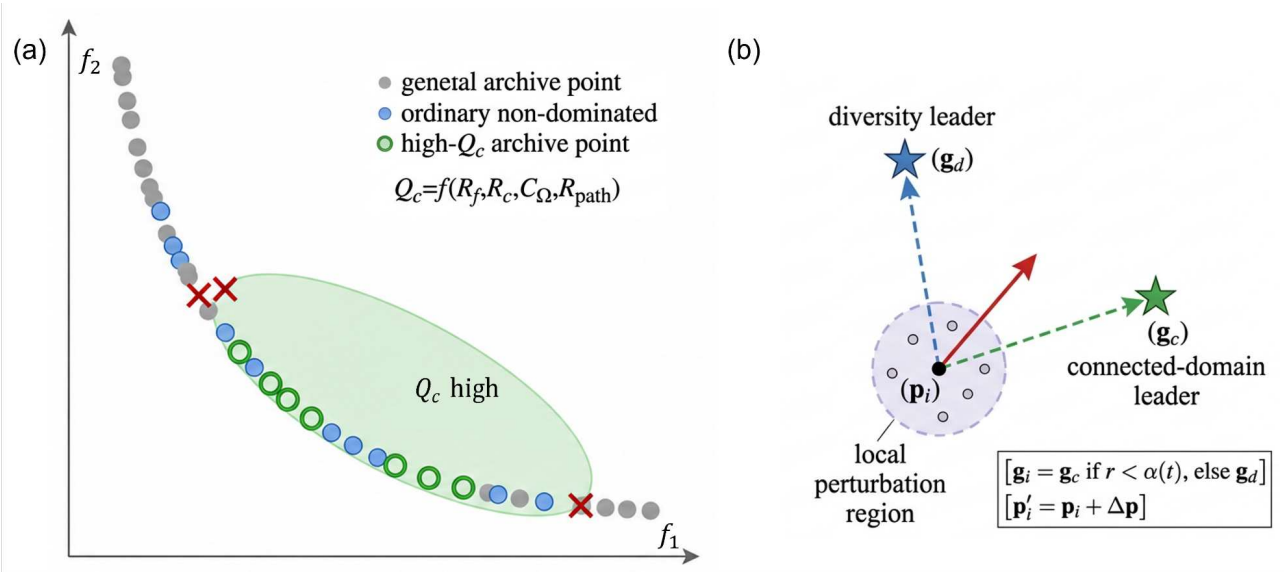


Figure 3. Connected-domain-guided archive and mixed-leader strategy.

Mechanism-derived constrained sizing model

For a fixed mechanism topology, the design vector is denoted by

$$\mathbf{p} = [p_1, p_2, \ldots, p_d]^T \in \mathscr{P}, \tag{1}$$

where $\mathscr{P} = [\mathbf{p}_{\mathrm{lb}}, \mathbf{p}_{\mathrm{ub}}]$ is the dimensional design box. The variables may represent link lengths, offsets or actuator-installation parameters depending on the fixed topology. During optimization, the topology is fixed; only the dimensional parameters are varied. This separation is useful because topology design and dimensional synthesis usually require different modeling and validation procedures.

The active input vector is

$$\mathbf{q} = [q_1, q_2]^T \in \Omega_q. \tag{2}$$

For each candidate design and input, passive coordinates or internal configuration variables $\mathbf{x}$ are obtained from the loop-closure equation

$$\boldsymbol{\Phi}(\mathbf{x}, \mathbf{p}, \mathbf{q}) = \mathbf{0}. \tag{3}$$

A solution is accepted only when the numerical residual is below the prescribed tolerance, the solution remains on the tracked assembly branch and all geometric limits are satisfied. Branch continuity is checked over neighboring input samples. Isolated valid samples that cannot be connected through neighboring usable samples are therefore distinguished from a continuously executable operating region.

Loop-closure failure, invalid geometry, invalid output, branch discontinuity and severe singularity risk mark an input sample as unusable. The effective mechanism workspace in the active-input representation is defined as

$$\Omega_{\mathrm{ECMW}}(\mathbf{p}) = \{\mathbf{q} \in \Omega_q^{\mathrm{grid}} \mid \boldsymbol{\Phi}(\mathbf{x}, \mathbf{p}, \mathbf{q}) = \mathbf{0},\ \text{valid},\ \text{continuous},\ \text{non-singular}\}. \tag{4}$$

On the discrete input grid, Ω_{ECMW} is decomposed into connected components. The feasible-sample ratio and largest connected-component ratio are

$$R_{\mathrm{f}}(\mathbf{p}) = \frac{|\Omega_{\mathrm{ECMW}}(\mathbf{p})|}{|\Omega_q^{\mathrm{grid}}|}, \qquad R_{\mathrm{c}}(\mathbf{p}) = \frac{|\mathscr{C}_{\max}(\mathbf{p})|}{|\Omega_q^{\mathrm{grid}}|}, \tag{5}$$

where $\mathscr{C}_{\max}$ is the largest usable connected component. The path-connectivity descriptor R_{path} is computed as the fraction of prescribed operating-region pairs that remain connected within $\mathscr{C}_{\max}$. Thus, a design can have a reasonable feasible-sample ratio but a poor R_{path} if the usable samples are split into disconnected islands.

The task output is denoted by $\mathbf{y}(\mathbf{p}, \mathbf{q})$. In the investigated mechanism, the optimization target is based on coverage in the sweep-angle-area task plane. With target task envelope Ω_T, the coverage metric is

$$C_{\chi A}(\mathbf{p}) = \frac{N_{\mathrm{occ}}(\Pi_{\chi A}[\Omega_u(\mathbf{p})] \cap \Omega_T)}{N_{\mathrm{grid}}(\Omega_T)}, \tag{6}$$

where $\Omega_u(\mathbf{p}) = \{\mathbf{y}(\mathbf{p}, \mathbf{q}) \mid \mathbf{q} \in \Omega_{\mathrm{ECMW}}(\mathbf{p})\}$, $\Pi_{\chi A}$ is the projection onto the sweep-angle-area plane and N_{occ} counts occupied target-envelope grid cells.

Connected-domain quality is used as an internal search-guidance score:

$$Q_{\mathrm{c}}(\mathbf{p}) = \eta_f \widehat{R}_{\mathrm{f}}(\mathbf{p}) + \eta_c \widehat{R}_{\mathrm{c}}(\mathbf{p}) + \eta_\chi \widehat{C_{\chi A}}(\mathbf{p}) + \eta_p \widehat{R_{\mathrm{path}}}(\mathbf{p}), \qquad \eta_f + \eta_c + \eta_\chi + \eta_p = 1, \tag{7}$$

where hats denote min–max normalized quantities under the same evaluation protocol. The weights $\eta_f, \eta_c, \eta_\chi$ and η_p are fixed across all compared algorithms. Treating Q_{c} as a guidance descriptor rather than as a third objective prevents the Pareto relation from retaining weak-coverage or high-load candidates solely because their connectivity score is favorable.

A reduced-coordinate quasi-static load proxy is computed from the task-space load $\mathbf{w}$ and the reduced task Jacobian $\mathbf{J}_r$, evaluated after loop-closure constraints have been satisfied:

$$\boldsymbol{\tau}_{\mathrm{proxy}} = \mathbf{J}_r^T \mathbf{w}. \tag{8}$$

The normalized load metric is clipped to reduce domination by extreme penalty values:

$$L_{\mathrm{clip}}(\mathbf{p}) = \min\{L_{\mathrm{norm}}(\mathbf{p}), L_{\max}\}. \tag{9}$$

The bi-objective optimization model is

$$\min_{\mathbf{p}\in\mathscr{P}} \mathbf{F}(\mathbf{p}) = \begin{bmatrix} 1 - C_{\chi A}(\mathbf{p}) \\ L_{\text{clip}}(\mathbf{p}) \end{bmatrix}. \tag{10}$$

Hard and soft violation scores are separated. In the implemented comparison, hard violations aggregate non-negotiable failures,

$$V_{\text{h}}(\mathbf{p}) = n_{\text{fail}} + n_{\text{geom}} + n_{\text{out}} + n_{\text{nan}}, \tag{11}$$

where the terms count loop-closure failure, geometric invalidity, output invalidity and numerical failure on the input grid. The unweighted soft-violation score is written as

$$V_{\text{s}}^{0}(\mathbf{p}) = \rho_{\chi}\left[C_{\chi A}^{\min} - C_{\chi A}\right]_{+} + \rho_{c}\left[R_{\text{c}}^{\min} - R_{\text{c}}\right]_{+} + \rho_{p}\left[R_{\text{path}}^{\min} - R_{\text{path}}\right]_{+} + \rho_{\sigma}\left[\sigma^{\min} - \sigma_{\min}\right]_{+} + \rho_{L}\left[L_{\text{norm}} - L_{\text{soft}}\right]_{+}, \tag{12}$$

where $[z]_{+} = \max(z, 0)$, $\sigma_{\min}$ denotes the minimum singularity margin over usable samples and $\rho_{\cdot}$ are fixed normalization weights. The adaptive score used in comparison is

$$V_{\text{s}}(\mathbf{p}, t) = \lambda(t) V_{\text{s}}^{0}(\mathbf{p}), \tag{13}$$

where $\lambda(t)$ is a prescribed non-negative schedule. This equation states explicitly how the adaptive soft-constraint weight enters personal-best comparison and archive filtering.

FCD-MOPSO algorithm

FCD-MOPSO keeps the particle position, velocity, personal-best and external-archive structure of MOPSO. Particle velocity and position are updated by

$$\mathbf{v}_{i}^{t+1} = w\mathbf{v}_{i}^{t} + c_{1}r_{1}(\mathbf{p}best_{i}^{t} - \mathbf{p}_{i}^{t}) + c_{2}r_{2}(\mathbf{g}_{i}^{t} - \mathbf{p}_{i}^{t}), \tag{14}$$

$$\mathbf{p}_{i}^{t+1} = \text{clip}(\mathbf{p}_{i}^{t} + \mathbf{v}_{i}^{t+1}, \mathbf{p}_{\text{lb}}, \mathbf{p}_{\text{ub}}). \tag{15}$$

The mechanism-aware evaluation of a particle returns

$$\mathscr{E}(\mathbf{p}_{i}, t) = \{\mathbf{F}(\mathbf{p}_{i}), V_{\text{h}}(\mathbf{p}_{i}), V_{\text{s}}(\mathbf{p}_{i}, t), Q_{\text{c}}(\mathbf{p}_{i})\}. \tag{16}$$

Candidate comparison is hierarchical: lower V_{h} is preferred first, lower V_{s} second, Pareto dominance third, and Q_{c} or objective-space diversity is used as the final tie-breaker.

Archive maintenance merges the current archive and evaluated candidate set, removes hard-infeasible and penalty-contaminated candidates, and extracts the non-dominated set. If the archive exceeds its predefined size, the retention score is

$$\Psi_{k} = \omega_{D}\widetilde{D}_{\text{crowd},k} + \omega_{Q}\widetilde{Q}_{c,k}, \qquad \omega_{D} + \omega_{Q} = 1, \tag{17}$$

where $\widetilde{D}_{\text{crowd}}$ and $\widetilde{Q}_{c}$ are normalized crowding distance and connected-domain quality. The candidate with the smallest score is removed until the archive-size limit is satisfied. This score is applied only after infeasible and penalty-contaminated candidates have been filtered; it cannot retain hard-infeasible candidates.

Leader selection uses a mixed strategy. Let $\mathbf{g}_{d}$ denote a diversity leader selected by crowding or objective-space diversity, and let $\mathbf{g}_{c}$ denote a connected-domain leader selected according to Q_{c}. The leader for particle i is

$$\mathbf{g}_{i}(t) = \begin{cases} \mathbf{g}_{c}, & r < \alpha(t), \\ \mathbf{g}_{d}, & r \geq \alpha(t), \end{cases} \qquad r \sim U(0,1). \tag{18}$$

Local perturbation is applied near promising candidates by

$$\mathbf{p}_{i}' = \mathbf{p}_{i} + \boldsymbol{\varepsilon} \odot (\mathbf{p}_{\text{ub}} - \mathbf{p}_{\text{lb}}), \qquad \boldsymbol{\varepsilon} \sim U(-s, s), \tag{19}$$

followed by boundary repair. No algorithm uses high-fidelity inverse-dynamics information during optimization; inverse-dynamics data are reserved for post-verification.

Algorithm 1. Overall procedure of FCD-MOPSO

Input: design bounds $\mathbf{p}_{\mathrm{lb}}, \mathbf{p}_{\mathrm{ub}}$, input domain Ω_q, target envelope Ω_T, swarm size N, archive size N_A, maximum evaluation budget $NFE_{\max}$.
Output: external archive $\mathscr{A}$ and representative solution set $\mathscr{S}_{\mathrm{rep}}$.

Initialize particle positions $\{\mathbf{p}_i\}_{i=1}^{N}$ and velocities $\{\mathbf{v}_i\}_{i=1}^{N}$ within the design bounds.
Evaluate all particles by the mechanism-aware evaluation procedure.
Set $NFE \leftarrow N$, $\mathscr{P}_{\mathrm{cand}} \leftarrow \{\mathbf{p}_i\}_{i=1}^{N}$ and $\mathbf{p}best_i \leftarrow \mathbf{p}_i$.
Construct the initial archive $\mathscr{A} \leftarrow \textsc{UpdateArchive}(\emptyset, \mathscr{P}_{\mathrm{cand}}, N_A)$.
Set iteration counter $t \leftarrow 0$.
while $NFE < NFE_{\max}$ **do**
  Update $\lambda(t)$ and $\alpha(t)$; set $\mathscr{P}_{\mathrm{cand}} \leftarrow \emptyset$.
  for $i = 1$ to N **do**
    Select leader $\mathbf{g}_i \leftarrow \textsc{SelectLeader}(\mathscr{A}, \alpha(t))$.
    Update $\mathbf{v}_i$ and $\mathbf{p}_i$ using the PSO equations and boundary repair.
    Evaluate $\mathbf{p}_i$, add it to $\mathscr{P}_{\mathrm{cand}}$ and set $NFE \leftarrow NFE + 1$.
    Update $\mathbf{p}best_i$ by feasibility-first comparison.
    if $NFE \geq NFE_{\max}$, **break**.
  end for
  Update archive $\mathscr{A} \leftarrow \textsc{UpdateArchive}(\mathscr{A}, \mathscr{P}_{\mathrm{cand}}, N_A)$.
  Set $t \leftarrow t + 1$.
end while
Select representative solutions $\mathscr{S}_{\mathrm{rep}}$ from $\mathscr{A}$.
Return $\mathscr{A}$ and $\mathscr{S}_{\mathrm{rep}}$.

Algorithm 2. Feasibility-first comparison and archive update

Feasibility-first comparison$(\mathbf{p}_a, \mathbf{p}_b)$

Prefer the candidate with smaller V_{h}.
If hard violations are equal, prefer the candidate with smaller V_{s}.
If soft violations are equal, apply Pareto dominance on $\mathbf{F} = [1 - C_{\chi A}, L_{\mathrm{clip}}]^T$.
If neither candidate dominates, prefer larger Q_{c}; use diversity or random selection only for the final tie.

UpdateArchive$(\mathscr{A}, \mathscr{P}_{\mathrm{cand}}, N_A)$

Merge archive and candidate set: $\mathscr{B} \leftarrow \mathscr{A} \cup \mathscr{P}_{\mathrm{cand}}$.
Remove hard-infeasible and penalty-contaminated candidates from $\mathscr{B}$.
If $\mathscr{B} = \emptyset$, keep the least-violating candidates as a temporary archive and return.
Extract non-dominated set $\mathscr{B}_{\mathrm{nd}} \leftarrow \mathrm{ND}(\mathscr{B})$.
While $|\mathscr{B}_{\mathrm{nd}}| > N_A$, compute D_{crowd}, Q_{c} and Ψ_k, then remove the candidate with the smallest Ψ_k.
Return $\mathscr{B}_{\mathrm{nd}}$.

Inverse-dynamics post-verification

Representative designs are further checked by inverse dynamics after optimization. The verification follows the standard manipulator dynamics form[37,38]

$$\mathbf{M}(\mathbf{q})\ddot{\mathbf{q}} + \mathbf{H}(\mathbf{q}, \dot{\mathbf{q}}) = \boldsymbol{\tau} + \mathbf{d}, \tag{20}$$

where $\mathbf{q}$ denotes the independent input coordinates after loop-closure reduction, $\mathbf{M}$ is the reduced mass matrix, $\mathbf{H}$ contains Coriolis, centrifugal and gravitational terms, $\boldsymbol{\tau}$ is the generalized actuation input and $\mathbf{d}$ denotes external-load and disturbance contributions. The post-verification reports peak force, RMS force, maximum force gradient and a force-smoothness index. These quantities are not fed back into the optimizer and therefore provide an independent engineering check on the selected representatives.

Experimental protocol and statistical analysis

All compared algorithms use the same design bounds, input scanning grid, task envelope, loop-closure solver, singularity criterion and load-proxy calculation. The algorithms are terminated under the same limited evaluation protocol. Repeated stochastic runs are conducted under a common random protocol; matched-run comparisons are used where appropriate.

Valid rate denotes the proportion of runs that return a non-penalty effective result under the soft-constrained benchmark. HQ rate denotes the proportion of all repeated runs that return a non-penalty representative satisfying the coverage, connected-domain and load-proxy quality criteria. Force-aware HQ is a subset of HQ runs and additionally satisfies the force-risk

condition. Penalty rate denotes the proportion of runs whose final result is penalty-contaminated or lacks an effective archive representative. These rates are reported alongside run-level diagnostics because a low-budget constrained run can fail by returning no usable non-penalty representative; such failures are not hidden by averaging only over successful runs. Conversely, a valid run is not necessarily a strictly feasible engineering design.

Optimization-quality indicators include $C_{\chi A}$, hypervolume (HV), L_{clip} and R_{c}. Search-process indicators include area-under-curve values for coverage, non-penalty archive ratio and penalty ratio, as well as first-hit evaluation progress for non-penalty and HQ candidates. Non-parametric sign tests and Wilcoxon signed-rank tests are used for matched comparisons to avoid strong normality assumptions in small-sample stochastic optimization comparisons[39,40]. For inverse-dynamics post-verification, PSO representatives were selected using both balanced and coverage-oriented criteria, so that force-response risks could be compared under different representative-selection preferences.

Results

The results are organized to match the proposed method and verification protocol. First, the active-input domain is examined to explain why a soft-constrained stress interpretation is required. Second, Basic MOPSO, FCD-MOPSO, PSO and GA are compared under the same limited evaluation protocol. Third, search-history and neighboring-envelope diagnostics are used to assess whether the improvement is only a final-value effect. Finally, ablation and inverse-dynamics post-verification are used to interpret representative engineering risk.

Input-domain risk map and feasibility diagnosis

Figure 4 compares representative Basic MOPSO and FCD-MOPSO designs in the active-input domain. The FCD-MOPSO representative produces 87 usable input samples out of 130 and a largest connected component of 52 samples, whereas the Basic MOPSO representative produces 85 usable samples and a largest component of 49 samples. The absolute increase in the largest connected component is therefore small, but it occurs together with lower maximum condition-number risk, lower peak load-proxy risk and lower force-gradient proxy in the displayed risk maps. This result provides representative-level evidence that connected-domain guidance can select a more executable region, without implying improvement in every grid-level descriptor or every run.

Strict-feasibility diagnosis showed that the absence of strictly feasible runs was dominated by task-envelope coverage pressure, with no dominant kinematic or load-transfer failure mode observed. Coverage violation appeared in all 80 diagnostic runs, with mean, median and maximum violation values of 0.0992, 0.0984 and 0.1053. Sweep-range violation appeared in 34 of 80 runs. Singularity-margin violation appeared in 76 of 80 runs but was numerically small, with a mean of 4.62×10^{-5}. Condition-number, load and force-gradient strict violations were absent in the diagnostic records. The following rate indicators are therefore soft-constrained non-penalty success measures. They are not equivalent to strict feasibility of a final engineering design.

Main low-budget benchmark comparison

Table 1 summarizes the main benchmark comparison. Relative to Basic MOPSO, FCD-MOPSO increases the valid-run rate from 0.6 to 0.8, the high-quality (HQ) rate from 0.1 to 0.4 and the force-aware HQ rate from 0.1 to 0.4. The penalty rate is reduced from 0.4 to 0.2. These changes indicate that the main benefit over Basic MOPSO is more stable formation of a non-penalty archive and a higher frequency of representative runs that satisfy the prescribed soft quality conditions.

Table 1. Low-budget baseline comparison under the same evaluation protocol.

Algorithm	Valid	HQ	Force-aware HQ	Penalty	Median $C_{\chi A}$	Median HV	Median L_{clip}	Median R_{c}
Basic MOPSO	0.6	0.1	0.1	0.4	0.0231	0.0200	4.83×10^{-4}	0.577
FCD-MOPSO	0.8	0.4	0.4	0.2	0.0243	0.0350	5.08×10^{-4}	0.615
PSO	0.8	0.4	0.4	0.2	0.0251	0.0450	5.65×10^{-4}	0.631
GA	0.6	0.1	0.1	0.4	0.0228	0.0300	4.79×10^{-4}	0.581

The PSO baseline reaches the same valid, HQ and force-aware HQ rates as FCD-MOPSO and has slightly higher median $C_{\chi A}$, median HV and median R_{c}. This comparison rules out a stronger claim of universal superiority. The value of FCD-MOPSO is narrower: it improves the archive-based multi-objective framework relative to Basic MOPSO while retaining a set of candidates from which coverage-preferred, balanced and force-aware representatives can be selected. PSO can converge rapidly to a coverage-oriented region under a low budget, but it does not maintain an external non-dominated archive and therefore provides less structural information for representative selection.

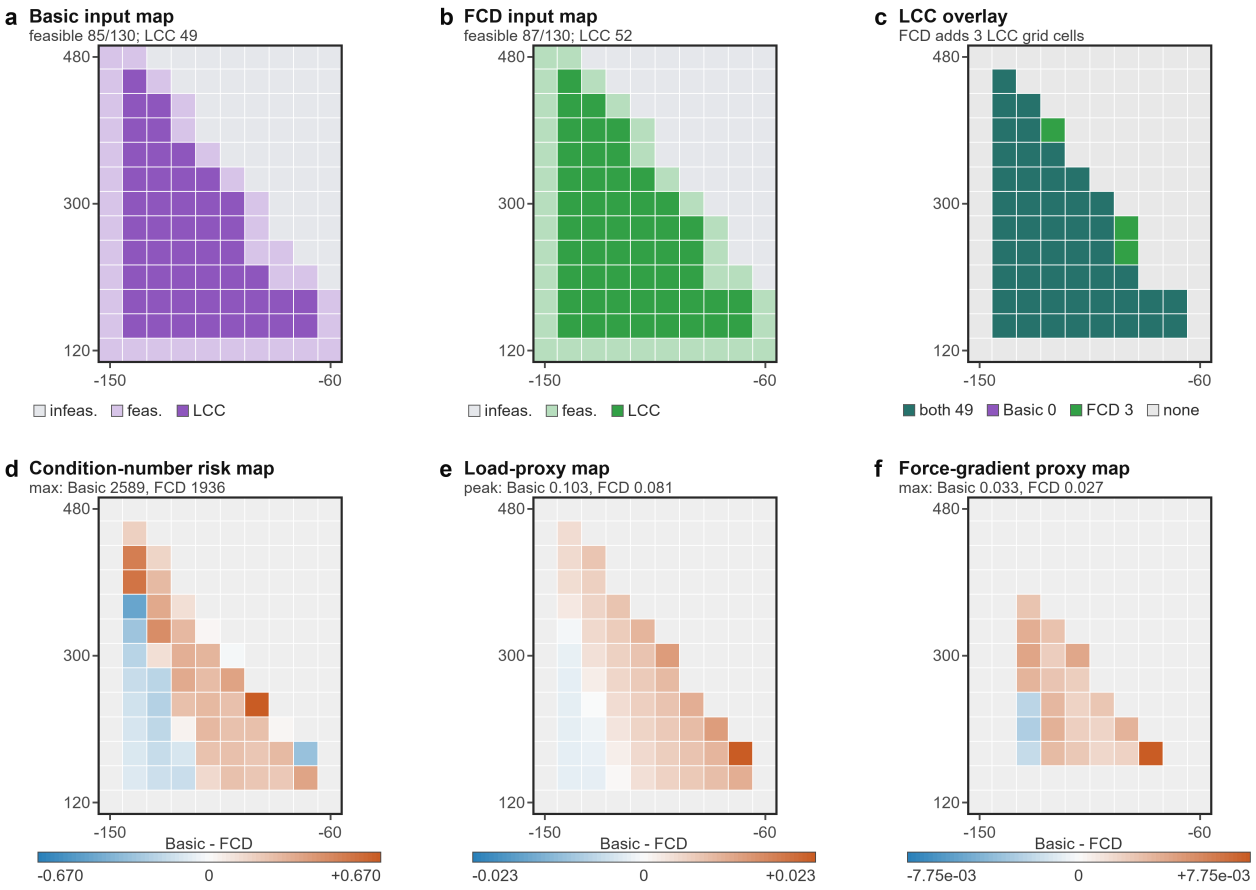


Figure 4. Input-domain engineering-risk map for the reference constrained sizing problem.

The median clipped load proxy of FCD-MOPSO is slightly higher than that of Basic MOPSO and GA in Table 1; therefore final scalar summaries alone are not sufficient to support the engineering interpretation. The subsequent inverse-dynamics verification is used as a post-optimization consistency check. This separation is important because the optimizer uses only the clipped load proxy during search, whereas the force histories are obtained from a richer verification model after optimization.

Search stability and neighboring stress settings

Search-process diagnostics showed that FCD-MOPSO formed usable archive states earlier than Basic MOPSO. The area under the $C_{\chi A}$ history increased from 0.0297 to 0.0317, the area under the non-penalty archive ratio increased from 0.3250 to 0.6250, and the area under the penalty ratio decreased from 0.3750 to 0.1750. The median first non-penalty hit advanced from 85.0 to 65.0 evaluations, and the median first HQ hit advanced from 170 to 95.0 evaluations. For a low-budget mechanism-synthesis run, this first-hit behavior is practically relevant because a late non-penalty hit leaves little remaining budget for archive refinement. Since MOPSO repeatedly samples leaders from the archive, early archive quality directly affects the direction of later particle updates.

Neighboring task-envelope stress tests further indicated that the coverage improvement was not produced by a single isolated target-envelope parameterization. For the matched-run difference $\Delta C_{\chi A}$, all three neighboring settings produced a positive/negative/tie pattern of 9/1/0 with a sign-test value of $p = 0.0215$. Auxiliary connected-domain and valid-weighted metrics showed weaker evidence: the largest connected-component ratio produced 7/1/2 with $p = 0.0703$, valid-weighted $C_{\chi A}$ produced 5/0/5 with $p = 0.0625$, and valid-weighted R_c produced 4/0/6 with $p = 0.1250$. The defensible conclusion is therefore limited to more consistent task-envelope coverage and earlier non-penalty archive formation, without supporting independent statistical improvement in every auxiliary descriptor.

Ablation and representative engineering verification

Figure 5 summarizes the ablation evidence. Full FCD-MOPSO, the variant without connected leader and the variant without hybrid archive remain FCD-like in the primary stress rates. Removing local perturbation reduces the valid, HQ and force-aware HQ rates toward the Basic MOPSO level. In the targeted ablation setting, full FCD-MOPSO improves $C_{\chi A}$ over Basic MOPSO with a positive/negative/tie pattern of 9/1/0, median difference 7.72×10^{-4}, sign-test $p = 0.02148$ and Wilcoxon signed-rank $p = 0.03711$. The same coverage signature for the no-connected-leader and no-hybrid-archive variants indicates that their independent benefits are not fully separated under the present low-budget protocol. Local perturbation is the clearest isolated contributor in the current ablation evidence.

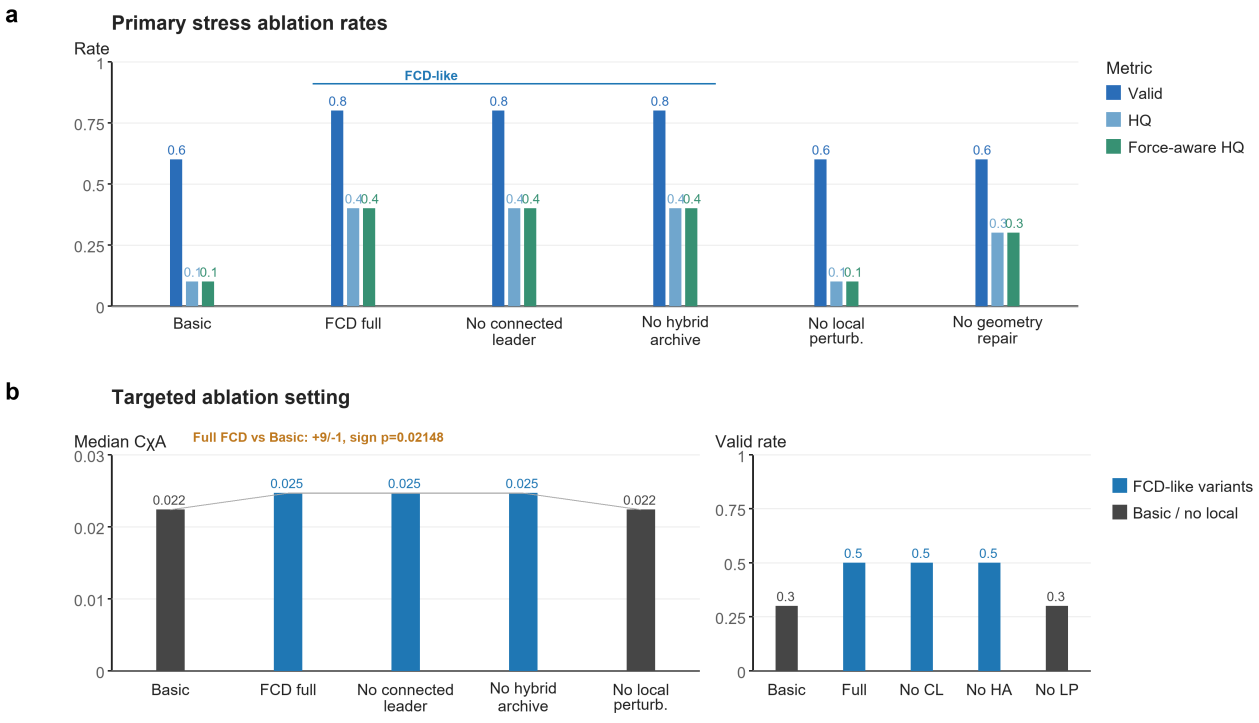


Figure 5. Ablation results for the FCD-MOPSO components.

This behavior is consistent with the fragmented input-domain landscape. When valid samples form narrow connected regions, a purely social-learning-driven update may overshoot or repeatedly cross invalid boundaries. A small bounded perturbation around promising candidates provides additional local sampling near these boundaries and can help the swarm locate neighboring usable cells. The connected-domain leader and hybrid archive are retained because they are structurally consistent with the mechanism-domain guidance objective, although their separate statistical effects are not resolved by the present low-budget ablation.

Representative inverse-dynamics force histories are shown in Fig. 6, and risk summaries are shown in Fig. 7. At the representative-solution level, FCD-MOPSO has lower maximum condition number than Basic MOPSO (1936 versus 2589), lower peak load-proxy map value (0.081 versus 0.103) and lower maximum force-gradient proxy (0.027 versus 0.033). In inverse-dynamics verification, FCD-MOPSO also has lower total peak force (1124 N versus 1199 N), lower total RMS force (549 N versus 610 N), lower maximum force gradient (1243 N/s versus 2376 N/s) and lower force-smoothness index (1.11 versus 1.98). The two PSO representatives show substantially larger force-gradient and force-smoothness risks despite competitive objective-space indicators.

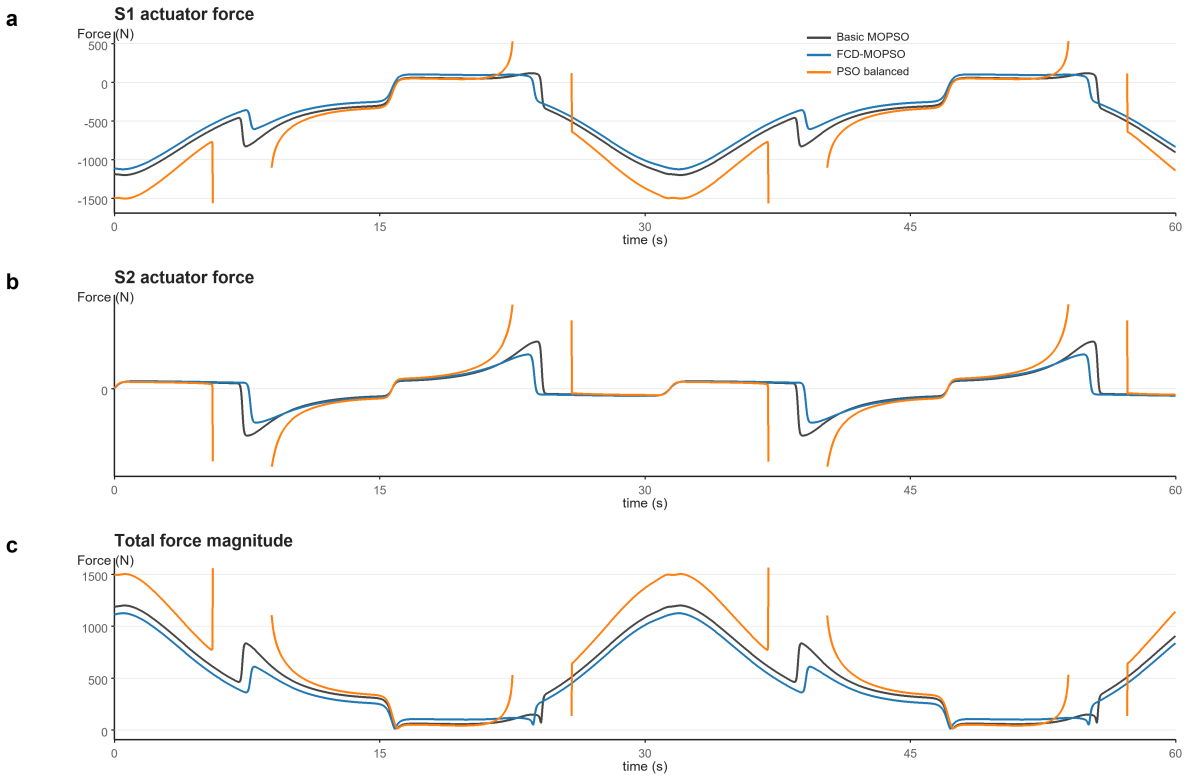


Figure 6. Inverse-dynamics force histories of representative designs.

The representative-level verification does not convert FCD-MOPSO into a dynamics optimizer. It only tests whether the representative selected from the proxy-guided archive enters an undesirable force-response regime when checked by a higher-fidelity model. The force-history results suggest that connected-domain and load-proxy guidance can improve representative quality beyond what is visible in a two-dimensional objective plot. This evidence remains post-verification evidence; dynamic optimality is outside the present optimization claim.

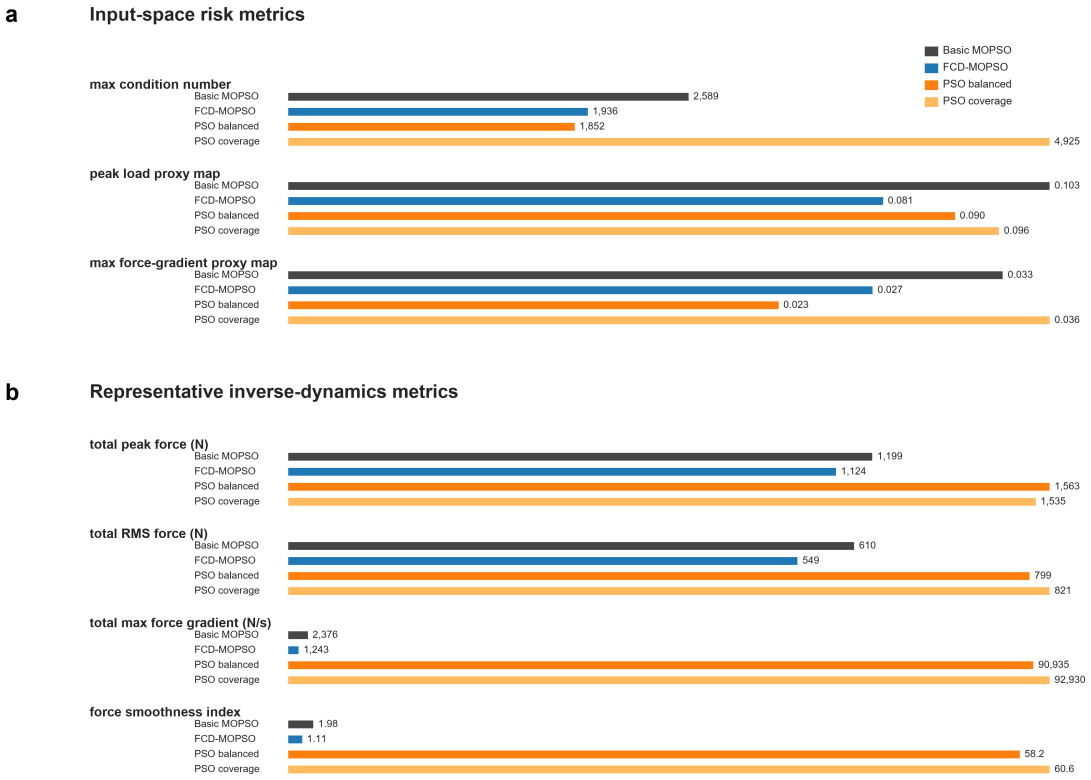


Figure 7. Engineering-risk summary for representative designs.

Discussion

The results support FCD-MOPSO as a mechanism-aware modification of archive-based MOPSO for fragmented feasible input domains. The mechanism-aware evaluation step converts each candidate dimension vector into a structured active-input state map rather than a single penalized objective vector. Feasibility-first comparison prevents objective-space dominance from overriding loop-closure failure, invalid geometry or discontinuous branch behavior. Archive filtering and hybrid retention reduce the probability that hard-infeasible, penalty-contaminated or weakly connected candidates become social leaders. Mixed leader selection and local perturbation provide the final link between objective-space diversity and input-space executability.

The strict-feasibility diagnosis determines the scope of the interpretation. The absence of strict feasibility is dominated by task-envelope coverage pressure, while condition-number, load and force-gradient strict violations are absent in the diagnostic records. The valid-run rate used in the main comparison is therefore a soft-constrained non-penalty success rate, not a strict feasibility rate. This distinction is important because the proposed method is evaluated as a low-budget screening optimizer for mechanism synthesis, where the first requirement is to avoid penalty-contaminated archive states and to recover representative candidates that remain meaningful under higher-fidelity verification.

The comparison with PSO limits the claim. PSO is competitive in valid rate, HQ rate, median coverage, hypervolume and largest connected-component ratio. FCD-MOPSO does not dominate PSO on all scalar indicators. Its value lies in preserving a multi-objective archive while using connected-domain quality to make the archive more informative for mechanism synthesis. The contrast between competitive objective-space indicators and higher force-history risk in the PSO representatives shows why mechanism-derived optimization cannot be judged only by generic objective-space indicators. For a closed-loop mechanism, an acceptable representative must cover the task envelope, remain continuously executable in the active-input domain and avoid undesirable force-response amplification.

The ablation results identify local perturbation as the clearest isolated contributor under the present evaluation budget. This does not make the connected-domain leader or hybrid archive redundant. Their effects are coupled with feasibility-first comparison and perturbation because all these components influence which candidates enter the archive and where the swarm samples next. The current evidence supports the complete FCD-MOPSO framework as a coherent mechanism-aware strategy; the independent effects of the archive and leader components are not separated by the current ablation design.

The framework differs from simple penalty-based constraint treatment in three ways. First, hard and soft violations are

separated before Pareto comparison, so numerical failure and small soft-margin shortage do not receive the same treatment. Second, connected-domain quality is retained even though it is not one of the two optimization objectives. Third, the archive is used not only to store objective-space non-dominated candidates but also to retain candidates that are more likely to be continuously executable over the active-input domain. These features are relevant for mechanisms in which similar output coverage can be generated by input domains with different connectivity, branch-continuity and force-transfer properties.

The present scope is a two-input planar multi-loop mechanism class with a discretized task-envelope coverage metric and a proxy-based load objective. Complete inverse dynamics is used for representative verification and is not fed back into the search objective. The repeated-run evidence is designed to expose low-budget constrained-search behavior rather than to constitute a broad benchmark over standard constrained multi-objective test suites. Other morphing or reconfigurable mechanisms may require aerodynamic, structural, thermal or control-oriented performance variables in addition to the kinematic and load-transfer descriptors used here.

Conclusion

This study proposed FCD-MOPSO for constrained dimensional synthesis of multi-loop mechanisms with fragmented feasible active-input domains. The method retains the particle update and external archive structure of MOPSO, but embeds mechanism-aware input-space evaluation, hierarchical feasibility comparison, connected-domain-guided archive maintenance, mixed leader selection and bounded local perturbation into the search loop. The connected-domain descriptor is not treated as an additional objective; it is used as a guidance signal that shapes comparison, retention and leader selection.

Under the investigated soft-constrained low-evaluation-budget protocol, FCD-MOPSO improved the non-penalty valid-run rate, HQ rate and force-aware HQ rate relative to Basic MOPSO. It also produced earlier non-penalty archive formation and more consistent coverage accumulation across neighboring task-envelope settings. Representative inverse-dynamics verification showed lower peak force, RMS force, force-gradient risk and force-smoothness index than the Basic MOPSO and PSO representatives. These findings indicate that mechanism-domain information can improve the engineering relevance of archive-based multi-objective search when the feasible input domain is fragmented.

The strict coverage target remains the dominant unresolved constraint in the diagnostic benchmark, and the reported success rates are therefore soft-constrained screening indicators rather than strict feasibility certificates. The contribution of FCD-MOPSO is the formation of more reliable mechanism-aware candidate archives and lower-risk representatives for subsequent engineering assessment within the same synthesis workflow.

Reporting and reproducibility statements

No human participants, human tissue, animals or biological materials were involved in this study.

Data availability

The numerical data generated and analyzed in this study, including run-level summaries, representative-solution metrics and source data for the figures, are available from the corresponding author upon reasonable request for academic verification. Access to mechanism-specific geometric data is restricted by institutional confidentiality requirements.

Code availability

The custom optimizer implementation and figure-generation scripts are available from the corresponding author upon reasonable request for academic verification. Release of mechanism-specific geometry modules is subject to institutional confidentiality requirements.

References

1. Gosselin, C. & Angeles, J. Singularity analysis of closed-loop kinematic chains. *IEEE Trans. Robot. Autom.* **6**, 281–290, doi: 10.1109/70.56660 (1990).
2. Gosselin, C. & Angeles, J. A global performance index for the kinematic optimization of robotic manipulators. *J. Mech. Des.* **113**, 220–226, doi: 10.1115/1.2912772 (1991).
3. Park, F. C. & Kim, J. W. Singularity analysis of closed kinematic chains. *J. Mech. Des.* **121**, 32–38, doi: 10.1115/1.2829437 (1999).
4. Bonev, I. A. & Gosselin, C. M. Singularity loci of planar parallel manipulators with revolute joints. *Electron. J. Comput. Kinemat.* **1**, 1–17 (2002).

5. Merlet, J.-P. *Parallel Robots* 2nd edn. (Springer, Dordrecht, 2006).
6. Yoshikawa, T. Manipulability of robotic mechanisms. *Int. J. Robot. Res.* **4**, 3–9, doi: 10.1177/027836498500400201 (1985).
7. Huang, T., Li, M., Li, Z. X., Chetwynd, D. G. & Whitehouse, D. J. Optimal kinematic design of 2-DOF parallel manipulators with well-shaped workspace bounded by a specified conditioning index. *IEEE Trans. Robot. Autom.* **20**, 538–543, doi: 10.1109/TRA.2004.825271 (2004).
8. Bai, S. Optimum design of spherical parallel manipulators for a prescribed workspace. *Mech. Mach. Theory* **45**, 200–211, doi: 10.1016/j.mechmachtheory.2009.06.007 (2010).
9. Kelaiaia, R., Company, O. & Zaatri, A. Multiobjective optimization of a linear Delta parallel robot. *Mech. Mach. Theory* **50**, 159–178, doi: 10.1016/j.mechmachtheory.2011.11.004 (2012).
10. Wu, G. Multiobjective optimum design of a 3-RRR spherical parallel manipulator with kinematic and dynamic dexterities. *Model. Identif. Control* **33**, 111–122, doi: 10.4173/mic.2012.3.2 (2012).
11. Gao, Z., Zhang, D. & Ge, Y. Design optimization of a spatial six degree-of-freedom parallel manipulator based on artificial intelligence approaches. *Robot. Comput. Integr. Manuf.* **26**, 180–189, doi: 10.1016/j.rcim.2009.06.006 (2010).
12. Nabavi, S. N., Shariatee, M., Enferadi, J. & Akbarzadeh, A. Parametric design and multi-objective optimization of a general 6-PUS parallel manipulator. *Mech. Mach. Theory* **152**, 103913, doi: 10.1016/j.mechmachtheory.2020.103913 (2020).
13. Yang, C., Ye, W. & Li, Q. Review of the performance optimization of parallel manipulators. *Mech. Mach. Theory* **170**, 104725, doi: 10.1016/j.mechmachtheory.2022.104725 (2022).
14. Wang, X., Lin, Y., Cao, Y., Wu, M. & Sun, S. Design and multi-objective optimization of a novel 5-DOF parallel mechanism with two double-driven chains. *Robotica* **41**, 2829–2849, doi: 10.1017/S026357472300070X (2023).
15. Antonov, A. *et al.* Design optimization of a parallel–serial manipulator with parallel architecture. *Robotics* **13**, 176, doi: 10.3390/robotics13120176 (2024).
16. Schappler, M. *et al.* Dimensional synthesis of parallel robots using bilevel optimization and hierarchical constraints. *Robotics* **14**, 29, doi: 10.3390/robotics14030029 (2025).
17. Peng, S., Du, L., Che, L. & Jin, Z. Dimensional multi-objective optimization design for 2RPU-RPS parallel mechanism. *Robotica* **43**, 1087–1109, doi: 10.1017/S0263574724002182 (2025).
18. Wang, X. *et al.* Kinematic calibration of a 5-DOF double-driven parallel mechanism with the sub-closed loop on limbs. *Robotica* **42**, 3709–3730, doi: 10.1017/S0263574724001607 (2024).
19. Zhang, X., Rong, Y., Wang, H. & Zhang, S. Kinematics and dynamics analysis of a new 5-degrees of freedom parallel mechanism with two double-driven chains. *Machines* **13**, 419, doi: 10.3390/machines13050419 (2025).
20. Yang, C. *et al.* A hybrid algorithm for the dimensional synthesis of parallel manipulators. *Proc. Inst. Mech. Eng. Part C J. Mech. Eng. Sci.* doi: 10.1177/09544062241312870 (2025).
21. Kennedy, J. & Eberhart, R. Particle swarm optimization. In *Proceedings of ICNN'95 – International Conference on Neural Networks*, vol. 4, 1942–1948, doi: 10.1109/ICNN.1995.488968 (1995).
22. Shi, Y. & Eberhart, R. C. A modified particle swarm optimizer. In *Proceedings of the 1998 IEEE International Conference on Evolutionary Computation*, 69–73, doi: 10.1109/ICEC.1998.699146 (1998).
23. Deb, K., Pratap, A., Agarwal, S. & Meyarivan, T. A fast and elitist multiobjective genetic algorithm: NSGA-II. *IEEE Trans. Evol. Comput.* **6**, 182–197, doi: 10.1109/4235.996017 (2002).
24. Coello Coello, C. A. & Lechuga, M. S. MOPSO: A proposal for multiple objective particle swarm optimization. In *Proceedings of the 2002 Congress on Evolutionary Computation*, 1051–1056, doi: 10.1109/CEC.2002.1004388 (2002).
25. Coello Coello, C. A., Pulido, G. T. & Lechuga, M. S. Handling multiple objectives with particle swarm optimization. *IEEE Trans. Evol. Comput.* **8**, 256–279, doi: 10.1109/TEVC.2004.826067 (2004).
26. Reyes-Sierra, M. & Coello Coello, C. A. Multi-objective particle swarm optimizers: A survey of the state-of-the-art. *Int. J. Comput. Intell. Res.* **2**, 287–308 (2006).
27. Tripathi, P. K., Bandyopadhyay, S. & Pal, S. K. Multi-objective particle swarm optimization with time variant inertia and acceleration coefficients. *Inf. Sci.* **177**, 5033–5049, doi: 10.1016/j.ins.2007.06.018 (2007).
28. Coello Coello, C. A., Lamont, G. B. & Van Veldhuizen, D. A. *Evolutionary Algorithms for Solving Multi-Objective Problems* 2nd edn. (Springer, New York, 2007).

29. Deb, K. An efficient constraint handling method for genetic algorithms. *Comput. Methods Appl. Mech. Eng.* **186**, 311–338, doi: 10.1016/S0045-7825(99)00389-8 (2000).

30. Coello Coello, C. A. Theoretical and numerical constraint-handling techniques used with evolutionary algorithms: a survey of the state of the art. *Comput. Methods Appl. Mech. Eng.* **191**, 1245–1287, doi: 10.1016/S0045-7825(01)00323-1 (2002).

31. Mezura-Montes, E. & Coello Coello, C. A. Constraint-handling in nature-inspired numerical optimization: past, present and future. *Swarm Evol. Comput.* **1**, 173–194, doi: 10.1016/j.swevo.2011.10.001 (2011).

32. Chen, J. *et al.* Multi-objective particle swarm optimization algorithm for task allocation and archived guided mutation strategies. *Sci. Rep.* **15**, 15821, doi: 10.1038/s41598-025-99730-1 (2025).

33. Luo, Y., Liu, Y., Chen, J., Yang, J. & Yu, J. Multi-objective particle swarm algorithm based on angular segmentation archive and dynamic update tactics. *Sci. Rep.* **15**, 31012, doi: 10.1038/s41598-025-16539-8 (2025).

34. Chen, S., Liu, Y., Yang, J., Ouyang, A. & Yu, J. A multi-objective particle swarm algorithm based on hierarchical clustering reference point maintenance. *Sci. Rep.* **15**, 44751, doi: 10.1038/s41598-025-28750-8 (2025).

35. Zitzler, E. & Thiele, L. Multiobjective evolutionary algorithms: a comparative case study and the strength Pareto approach. *IEEE Trans. Evol. Comput.* **3**, 257–271, doi: 10.1109/4235.797969 (1999).

36. Miettinen, K. *Nonlinear Multiobjective Optimization* (Kluwer Academic Publishers, Boston, 1999).

37. Murray, R. M., Li, Z. & Sastry, S. S. *A Mathematical Introduction to Robotic Manipulation* (CRC Press, Boca Raton, 1994).

38. Siciliano, B., Sciavicco, L., Villani, L. & Oriolo, G. *Robotics: Modelling, Planning and Control* (Springer, London, 2009).

39. Wilcoxon, F. Individual comparisons by ranking methods. *Biom. Bull.* **1**, 80–83, doi: 10.2307/3001968 (1945).

40. Demšar, J. Statistical comparisons of classifiers over multiple data sets. *J. Mach. Learn. Res.* **7**, 1–30 (2006).

Author contributions statement

R.C. developed the optimization framework, implemented the numerical experiments, analyzed the results and drafted the manuscript. Z.Y. contributed to mechanism modeling, experimental design and result interpretation. H.S. supervised the study and revised the manuscript. S.M. and Z.W. contributed to data analysis, figure preparation and manuscript checking. All authors reviewed the manuscript.

Funding

This work was supported by the Natural Science Foundation of Zhejiang Province under Grant No. LY24E050004.

Additional information

Competing interests. The authors declare no competing interests. Correspondence and requests for materials should be addressed to H.S.